Nano Energy 56 (2019) 759–769

Contents lists available at ScienceDirect

Nano Energy

journal homepage: www.elsevier.com/locate/nanoen

Full paper

Self-organized and self-propelled aero-GaN with dual hydrophilic-hydrophobic behaviour

Ion Tiginyanu[a,b,c,*], Tudor Braniste[b], Daria Smazna[a], Mao Deng[a], Fabian Schütt[a], Arnim Schuchardt[a], Marion A. Stevens-Kalceff[d], Simion Raevschi[e], Ulrich Schürmann[a], Lorenz Kienle[a], Nicola M. Pugno[f,g,h], Yogendra Kumar Mishra[a,**], Rainer Adelung[a,**]

[a] Institute for Materials Science, Kiel University, Kaiserstr. 2, D-24143 Kiel, Germany
[b] National Center for Materials Study and Testing, Technical University of Moldova, Stefan cel Mare av. 168, MD-2004 Chisinau, Moldova
[c] Academy of Sciences of Moldova, Stefan cel Mare av. 1, MD-2001 Chisinau, Moldova
[d] School of Physics, University of New South Wales, 2052 Sydney, NSW, Australia
[e] Department of Physics and Engineering, State University of Moldova, Alexei Mateevici str. 60, MD-2009 Chisinau, Moldova
[f] Laboratory of Bio-Inspired and Graphene Nanomechanics, Department of Civil, Environmental and Mechanical Engineering, University of Trento, 38123 Trento, Italy
[g] School of Engineering and Materials Science, Queen Mary University of London, Mile End Road, E1 4NS London, United Kingdom
[h] Ket Lab, Edoardo Amaldi Foundation, Italian Space Agency, Via del Politecnico snc, 00133 Rome, Italy

ARTICLE INFO

Keywords:
Gallium nitride
Hollow tetrapods
3D network
Self-assembling tetrapods on water
Hydrophobic wetting
Hydrophilic dewetting

ABSTRACT

Nature utilizes hydrophilic-hydrophobic biomolecular entities to perform self-organized structural and functional tasks, including the formation of cellular compartments and motion, separation of chemicals or self-healing properties in a highly energy efficient manner. So far, no inorganic artificial micro/nanostructure units are known that self-organize and mimic such functions just by adding liquid. Here we develop the first nanomaterial exhibiting hydrophobic wetting and hydrophilic dewetting. Consisting of gallium nitride nanoscopically thin membranes shaped as hollow microtetrapods, which we term *aerogalnite* (AGaN), the nanomaterial is extremely porous, mechanically flexible, stretchable, and exhibits hydrophilicity under tension and hydrophobicity when compressed against water. Self-assembling the AGaN tetrapods on water enabled us to develop self-healing waterproof rafts carrying liquid droplets 500-times as heavy as rafts, and to demonstrate self-propelled liquid marbles exhibiting velocity of rotation as high as 750 rot/min. The specific force of the detachment of AGaN from the water surface was experimentally determined equal to 35 mN/cm^2. The new developed material aerogalnite and its peculiar characteristics are promising for applications in sensorics, microfluidic devices and microrobotics.

1. Introduction

The unique properties of biological cell membranes are conferred by the molecular building blocks – phospholipids that both attract and repel water [1,2]. The hydrophilicity of a phospholipid is generated by its head based on polar phosphate groups, while the hydrophobicity is caused by the nonpolar tail consisting of two *fatty acid* chains. When added to water, the phospholipids self organize without any energy input and form a bilayer, the hydrophobic tails of both layers clustering together, away from the water, with the hydrophilic heads facing the water. In such a way a separation layer is created that controls the energy flux between both sides [1,2]. So far, no inorganic artificial micro/nanostructures are known that exhibit dual hydrophobic-hydrophilic properties and can self-organize when interacting with water to mimic the functions of a cell membrane. In our attempts to identify technological solutions for building such artificial structures, we started with the following general considerations. First, an artificial robust entity that enables self-assembling into a membrane could be constructed in the shape of a tetrapod since micro/nanometer scale tetrapods, especially hollow ones, allow substantial elastic deformation [3–5]. Second, when the individual tetrapods are transferred on a flat surface, the first monolayer automatically assumes the "three arms down" position, thus by inducing floating tetrapods to group together on the water surface one can mimic the formation of a phospholipid bilayer, where the free ends of bottom and top arms would play the role of polar phosphate groups in the phospholipid bilayer, while the four

* Corresponding author at: Institute for Materials Science, Kiel University, Kaiserstr. 2, D-24143 Kiel, Germany.
** Corresponding authors.
E-mail addresses: tiginyanu@asm.md (I. Tiginyanu), ykm@tf.uni-kiel.de (Y.K. Mishra), ra@tf.uni-kiel.de (R. Adelung).

https://doi.org/10.1016/j.nanoen.2018.11.049
Received 1 June 2018; Received in revised form 6 November 2018; Accepted 17 November 2018
Available online 26 November 2018

arms of each tetrapod – the role of clustering together nonpolar tails. Third, taking into account the polar-nonpolar features, promising materials for building tetrapods could be chosen among inorganic semiconductors [6,7] exhibiting both polar and nonpolar crystallographic planes.

Gallium nitride (GaN), a wide-bandgap semiconductor compound (E_g = 3.4 eV at 300 K) which in the 1980s looked unpromising from the technological point of view, has in the last two decades registered a fascinating increase in the crystalline quality of epitaxial layers determining its leading role in the development of the modern solid-state lighting industry. The demonstration and successful commercialization of GaN-based blue light emitting diodes resulted in the physics Nobel Prize to I. Akasaki, H. Amano and S. Nakamura in 2014. Exhibiting an impressive number of unique properties such as high breakdown voltage, high switching frequencies, enhanced power efficiency, high electrical conductivity, excellent thermal stability and radiation hardness, GaN has been remarkably successful in the area of high-power/high-frequency electronic applications, and is now considered the second most important semiconductor material after silicon. In addition, GaN possesses pronounced piezoelectric properties which open new applied avenues towards nanogenerators, piezotronics, nano-electro-mechanical systems, micro-opto-electro-mechanical systems, etc. [8–11]. In particular, GaN nanowire arrays for high-output nanogenerators have been demonstrated [12–15], while GaN nanocrystalline layers deposited on graphene aerogel enabled the fabrication of a highly flexible ultra-lightweight pressure sensor [16]. Three dimensional flexible architectures for multifunctional applications have been recently fabricated by applying growth of GaN nano/micro-crystallites on the huge surfaces inherent to carbon based aerographite scaffolds [17,18].

In spite of the fact that some compounds semiconductor and other materials can be grown as tetrapods by direct synthesis [4,6,19,20], the geometrical shape involved is not inherent to direct growth of gallium nitride. It is to be noted, however, that epitaxial growth of single crystalline GaN was demonstrated previously on ZnO nanocolumns (due to extraordinary low lattice mismatch of ~1.8%) with simultaneous or subsequent removal of zinc oxide [21,22] which paves the possibility to grow any desired complex shaped hollow gallium nitride structures, for example, tetrapods, multipods, by adopting template based strategy. The sacrificial template based GaN growth sounds feasible, but it still has to overcome several requirements, such as availability of desired structural morphologies, easy techniques offering homogeneous deposition of GaN on the templates, and last but most challenging, the successful removal of the underneath template.

In this work, the flame made zinc oxide tetrapods were selected as sacrificial templates for the GaN deposition [19], For GaN growth, we show that the hydride vapor phase epitaxy (HVPE) technique offers controlled deposition of homogeneous thin layers under adequate technological conditions and subsequent removal of the underneath zinc oxide template. The GaN deposition combined with the template removal possibility enables one to fabricate GaN hollow microtetrapods which reveal on their inner surfaces nanoscale traces of crystalline zinc oxide with outstanding chemical stability. Like the hydrophilic claws of the flying water lily beetles [23,24], the free ends and internal walls of AGaN tetrapod arms are pinned to the water surface by sizeable cohesion which is experimentally determined. Accordingly, for the AGaN tetrapod arm ends and internal walls we derive an intrinsic contact angle of 82° resulting under tension to a perfectly 0° apparent contact angle; the external walls of the AGaN tetrapods (excluding arm ends) are hydrophobic with an intrinsic contact angle that we estimate as 93°, resulting under compression to an apparent contact angle of about 170°. Taking inspiration from both the ability of pond skaters to walk on water and the powerful grip of fire ants forming waterproof rafts during floods [25–28], we use AGaN networks to fabricate high-performance micro-hydrofoils with remarkable cargo capabilities and self-healing functionality. Furthermore, by encapsulating liquid droplets with AGaN networks, we demonstrate highly energy-efficient self-propelled liquid marbles exhibiting record velocity of rotation and highest known lifetime of translational motion, these artificial cell membranes being extremely robust in both chemistry and structure, e.g., withstanding ultrasound.

2. Experimental

2.1. Aerogalnite synthesis

The aerogalnite samples were produced by deposition of GaN thin films on sacrificial templates composed from highly porous ZnO networks of microtetrapods [19]. Growth of GaN was realized in a HVPE system equipped with a four-temperature-zone-heated horizontal reactor. Metallic gallium, ammonia (NH_3) gas, hydrogen chloride (HCl) gas and hydrogen (H_2) were used as source materials and carrier gases. In the source zone, GaCl was formed as a result of chemical reactions between gaseous HCl and liquid Ga at 850 °C. The GaCl and NH_3 gas reacted with each other in the react zone, where at the beginning the temperature was kept at 600 °C for 10 min to initiate nucleation of GaN on the surface of ZnO microtetrapods, and then increased up to T_g = 850 °C, 900 °C or 950 °C for durations up to 30 min to produce GaN layers with different thicknesses. In the process of GaN growth, the HCl, NH_3 and H_2 flow rates were equal to 15 sml/min, 600 sml/min and 3600 sml/min, respectively. Note that at the growth temperature T_g, along with GaN deposition, simultaneous gradual decomposition and removal of the underneath ZnO template occurs due to harsh reaction conditions at T_g.

2.2. Structural characterization

The microstructural evolutions of aerogalnite architecture were investigated by a Scanning Electron Microscopy (SEM) instrument Zeiss Ultra Plus. The compositional analysis of AGaN networks was carried out using Energy Dispersive X-ray (EDX), in combination with SEM and Transmission Electron Microscopy (TEM). TEM analysis was performed with a Tecnai F30 STwin electron microscope (300 kV, field-emission gun, spherical aberration constant Cs = 1.2 mm. Energy-filtered TEM (EFTEM) with a post-column Gatan Image Filter was used to obtain elemental maps of the sample.

2.3. Mechanical characterizations

The mechanical measurements were conducted with a self-designed/built computer-controlled setup which consists of a Kern PLE 310-3 N precision balance and a Märzhäuser Wetzlar HS 6-3 micromanipulator. The setup allows a stepwise tensile or compressive deformation of the sample up to an arbitrary number of cycles while the force is measured by the balance.

2.4. AGaN raft formation and liquid marbles

To fabricate AGaN rafts, the aerogalnite powder was sprinkled in a 10-mm diameter sapphire cylinder placed in a Petri dish partially filled in with water. The water bath with floating aerotetrapods was subjected simultaneously to ultrasound treatment in a Bandelin Sonorex ultrasound bath at 35 kHz and maximum output power of 120 W. As a result, a raft consisting of interpenetrating AGaN tetrapods was created which covered the whole surface of the water inside the sapphire cylinder. To release the raft from the cylinder, we added as much water to the Petri dish as to surpass the upper edge of the sapphire cylinder. Liquid marbles were fabricated using distilled water. For experiments related to self-propelled liquid marbles, we used a commercially available alcoholic solution with ingredients enabling to maintain the surface tension.

3. Results and discussion

3.1. Morphology, crystallinity and elasticity

Fig. 1a illustrates the morphology of the as-grown ZnO template, while Fig. 1b shows a comparison between an original zinc oxide template and a GaN grown at T_g = 850 °C for 10 min with simultaneous decomposition of the template. Notable colour change from white to yellow after GaN deposition is clearly visible (digital photographs in Fig. 1b) and the resultant new material is superhydrophobic with the contact angle of a water droplet of 170° (Fig. 1c). Fig. 1(d-i) shows the morphology of samples subjected to HVPE process taking place at 850 °C for two different periods of time. The sacrificial template is removed in both cases, although some traces of the zinc oxide survive as will be described below. Following this strategy, i.e., thin layer deposition and simultaneous removal of the template, we have successfully developed a highly porous three-dimensional architecture, entirely built out of hollow tetrapods referred as so called aerotetrapods. The wall thickness of the hollow aerotetrapod arm depends upon the deposition time in the HVPE process at T_g = 850 °C which can be tailored from around 15 nm (least) to few 100 nm depending upon the requirements as demonstrated by different AGaN variants shown in SEM images (Figs. 1f, 1i). Further increase of T_g leads to the formation of porous walls (Supplementary Information, Fig. S1). The morphological investigations (Fig. 1d-i) verify the proposed strategy that the thin GaN layers of desired thickness can be homogeneously deposited on a ceramic template which retains the morphological intactness of the ceramic template, even after template's removal. It is important to emphasize that the higher the growth temperature Tg, the higher the rate of decomposition of the underneath ZnO in the HVPE process. The etching of ZnO starts in the area of the tetrapod central joint where the epitaxial growth of GaN appears to occur at lower rates in comparison with the growth on the surface of the arms. With the reaction time, the ZnO etching proceeds in directions toward the free ends of the underneath arms, the extrusion of the products of etching reactions being realized through nano-micropores inherent to tetrapod the central joint. In some instances, the remnant ZnO can be easily detected in the areas of free ends of the arms, as illustrated by SEM images in Fig. S2 (Supplementary Information). Additionally, the experimental results demonstrated that it is almost impossible to coat ZnO tetrapods with GaN without at least partial removal of underneath ZnO.

Deposition of GaN and simultaneous removal of ZnO leads to drastic reduction in the overall density of the tetrapodal architecture, a conversion from filled to hollow geometry. The density of the AGaN sample shown in Fig. 1b (right) equals 12.3 mg/cm^3 which falls in the density range inherent to cellular materials [29]. The weight of the specimen involved (7.4 mg) is close to the weight of a couple of snowflakes. The AGaN architecture exhibits fascinating electromechanical coupling abilities which are confirmed by its energetic motions under applied electric fields. As shown in Section 1 of the Video (Supplementary Information), a specimen of AGaN placed in a glass tube jumps like a super-elastic micro-ball under the action of a spatially varying static

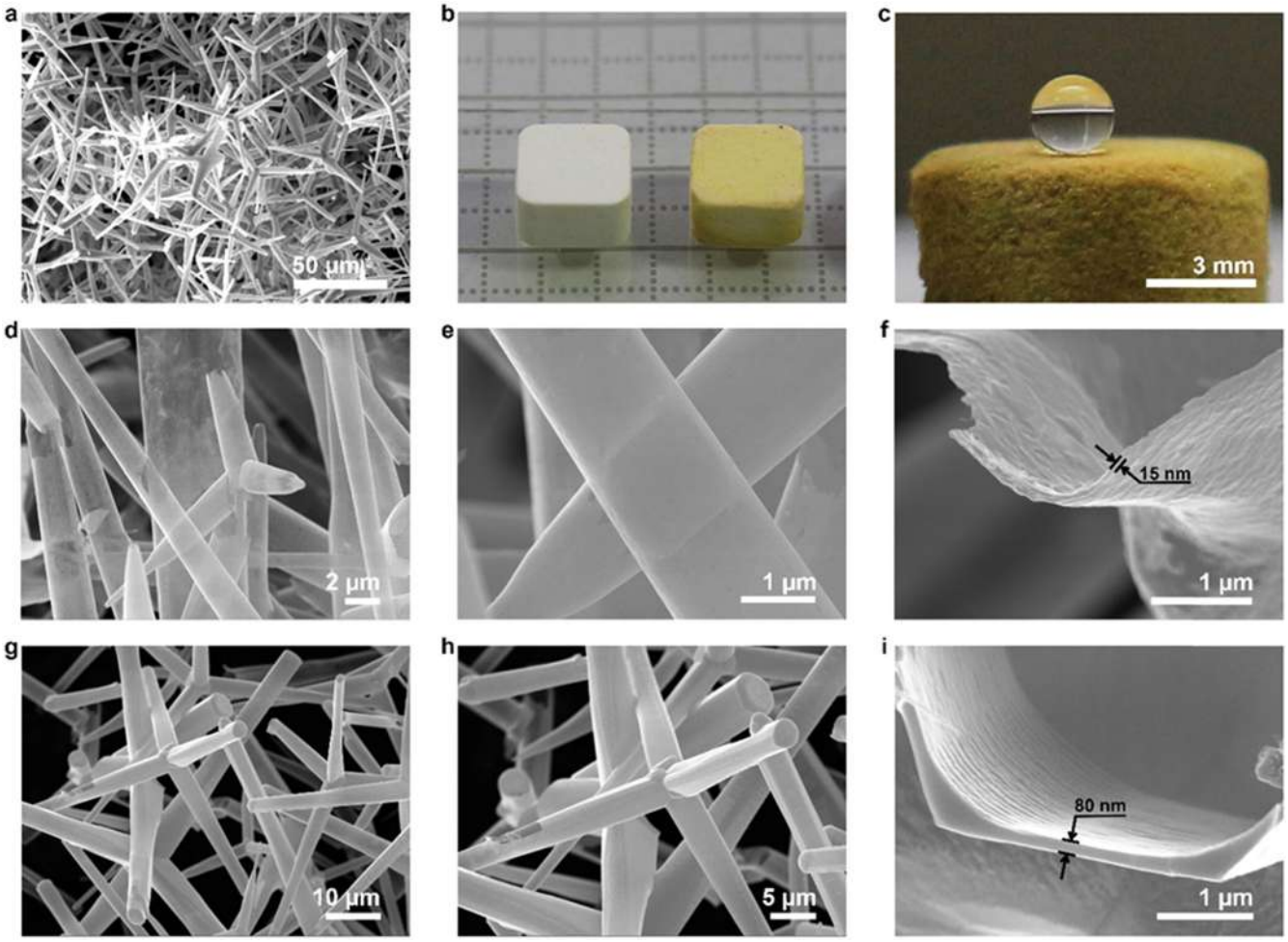

Fig. 1. (a) Morphology of the ZnO tetrapodal template. (b) Comparison between the original ZnO template (left) and a specimen subjected to GaN deposition at 850 °C with simultaneous decomposition of ZnO (right). (c) The AGaN tetrapodal network is superhydrophobic (in contrast to ZnO templates which are superhydrophilic). (d-i) SEM images corresponding to two differnet AGaN samples characterized by different durations of deposition at T_g = 850 °C.

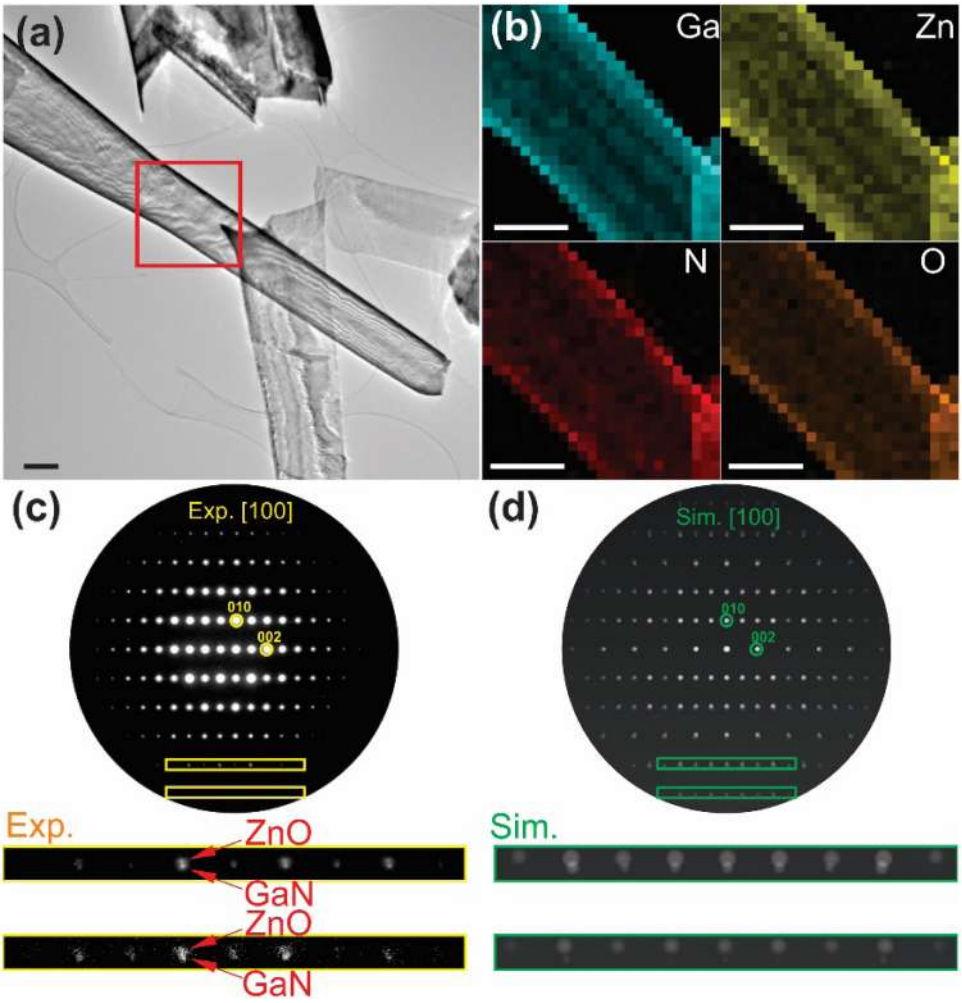

Fig. 2. Combined TEM chemical and structural analyses of the GaN (T_g = 850 °C) hollow microtubes with an amount of residual Zn around 7 at%. (a) TEM bright-field image of a GaN microtube; (b) EDX elemental maps from the red boxed region in (a). Blue: Gallium map; Red: Nitrogen map; Yellow: Zinc map; Orange: Oxygen map. (c) SAED pattern from the marked region in (a), showing a projection along the [100] zone axis of GaN or ZnO (space group: *P*63*mc*). (d) Computer simulated SAED pattern assuming an exact overlapping of the same [100] zone axis of both GaN and ZnO phases. In the bottom a comparison of two enlarged sections from the marked 4th and 5th order reflections in (c) and (d) is displayed. Scale bar is 500 nm.

electric field generated by a moving amber stick preliminarily rubbed with wool. This behaviour can be attributed to dielectrophoresis [30]. Note that the AGaN specimen continues its energetic motion several seconds after the removal of the electrically-charged stick, these are driven by the continuous distribution of charges.

Supplementary material related to this article can be found online at doi:10.1016/j.nanoen.2018.11.049.

Although the main part of the ZnO skeleton is removed in the process of GaN deposition, we found traces of ZnO on the inner surface of the GaN microtubular structures. Fig. 2 presents the results of combined chemical and structural analyses, realized using TEM, of AGaN deposited at 850 °C for 10 min. The TEM bright-field image taken from a GaN microtube (Fig. 2a) demonstrates that its wall represents a continuous layer of GaN. Besides, the microtube shows a high transparency to the electron beam, as another piece of the GaN film can be seen through it. A statistic EDX analysis in TEM mode from several GaN microtubes transferred on the grid shows an average amount of 7 at% of Zn remaining in the microstructures. To further reveal the spatial distribution of the residual Zn, a spatially more confined EDX elemental mapping was performed (see Fig. 2b). As can be inferred from the EDX map, Zn and O are present together with GaN, without any preferential aggregations on the inner wall of the microtube. Note that an atomic scale layer of ZnO found inside of the microtubes is utilized for the here intended applications, as ZnO is hydrophilic, while the outer GaN shell is hydrophobic.

Structural analysis with selected area electron diffraction (SAED) suggests the single crystallinity of the microtube walls (see Fig. 2c). However, when the projection of the crystal lattice is along the [100] axis, ZnO and GaN can be hardly distinguished in TEM, because the d-value of the ZnO (010) plane is only about 0.7 Å larger than that of GaN. Only for higher order Bragg reflections, a distinction between the two materials can be made, cf. splitting of the Bragg intensities in the experimental and simulated patterns of Fig. 2c and Fig. 2d. The enlarged view of the 4th and 5th order reflections on the bottom of Fig. 2 illustrates a d-value of the (010) plane (0.280 nm; the ZnO literature value is 0.281 nm [31]) determined from the inner circle, and another one calculated from the outer circle with a smaller d-value of 0.277 nm (comparable to the GaN literature value of 0.274 nm [32]). The enlarged regions marked with green boxes confirm a reasonable match with the experimental data. It can be speculated, on the one hand, that the residual ZnO might be serving as a stabilizing layer for the deposited GaN to grow with a similar lattice parameter and further achieve a highly crystalline epitaxial growth in a three-dimensional manner. On the other hand, GaN stabilizes the ZnO interface layer in a unique fashion as ZnO usually decomposes under hydrogen treatment.

The amount of residual ZnO on the inner surface of hollow tetrapods can be reduced down to 3–4 at% (from EDX results) by increasing T_g up to 950 °C (Fig. 3a-c). Note that, although the walls of the hollow GaN microtetrapods grown at 950 °C are porous, they exhibit a single crystalline structure (see SAED in Fig. 3d). The pronounced porosity of the walls at the growth temperature T_2 = 950 °C may be attributed to intense decomposition and removal of the ZnO template. To further reduce the amount of residual Zn from the AGaN architecture, a series of samples was subjected to a post-growth treatment in hydrogen atmosphere. Fig. 3e-f illustrate typical morphologies inherent to samples grown at 850 °C with subsequent treatment in hydrogen atmosphere at

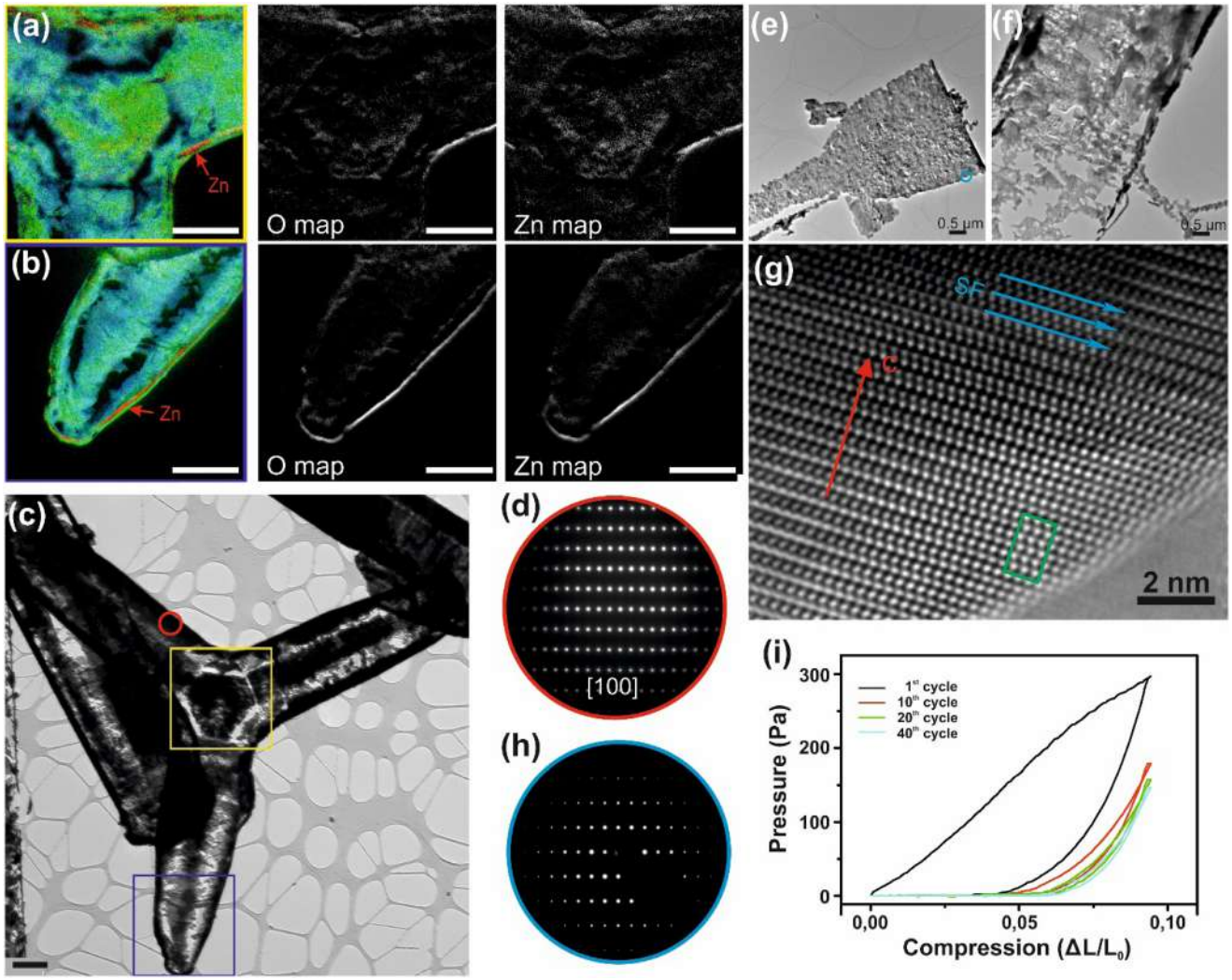

Fig. 3. TEM and EFTEM investigation of hollow AGaN tubes. (a-b) EFTEM elemental maps from the yellow and the blue marked regions (see TEM bright-field image in (c)) of the porous GaN tetrapod (T_g = 950 °C). The elements of interest in the EFTEM maps are represented with different colors (Ga: Green, Zn: Red, N: Blue). Additionally, the O and Zn maps are given. Scale bar is 1 μm. (d) SAED pattern recorded from the red circled area (see TEM bright-field image in (c)) on the tetrapod arm. (e-f) TEM micrographs from two particles of the AGaN sample after H_2 treatment showing very porous morphology. (h) SAED pattern acquired from the blue circle region in (e) which is indexed to be along the [100] zone axis of GaN. (g) HRTEM micrograph recorded on the edge of a hole in the particle shown in (e). The red arrow indicates the c-axis of the crystal lattice. Some stacking faults are marked out with blue arrows. A multislice computer simulation image is inserted for comparison with the experimental data (defocus Δf = 70 nm, sample thickness t = 4.74 nm). (i) Compressive stress – strain response of the AGaN network under 40 loading and unloading cycles.

900 °C suggesting that the hydrogen treatment removed most of the remaining Zn (EDX: 0.7 at%) and partially etched the GaN, too. SAED investigation (Fig. 3h) shows no more splitting of the Bragg intensities in comparison with the results illustrated in Fig. 2c. Nevertheless, the high-resolution TEM (HRTEM) micrograph conducted on a smaller region in the highly crystalline particle (Fig. 3e) revealed some stacking faults (intrinsic type I_1 basal-plane stacking faults inherent to the wurtzite structure [33,34]) arranged perpendicular to the crystallographic c-axis (see Fig. 3g). The simulation (green box in Fig. 3g) confirms the wurtzite structure of GaN. Thus, the architecture of AGaN consists of hollow microtetrapods with arm diameters of several micrometers and follows the spatial architecture of the ceramic template. Nanoscopic ZnO was observed to be remaining at the inner surface of GaN walls after the HVPE process, which is mainly due to a '*partner-induced chemical stability*' phenomenon, as an ultrathin ZnO film is shielded during the HVPE process because of strong chemical binding at the interfaces.

Despite of very low density, the fabricated 3D architecture of mutually interpenetrated GaN aerotetrapods is mechanically flexible as confirmed by cyclic loading and unloading stress (compressive) – strain response presented in Fig. 3i. The behaviour under the first loading-unloading cycle discloses sizeable plastic deformation (Fig. 3i, curve 1) which is related to the hierarchical architecture of the AGaN consisting of partially interpenetrated gallium nitride aerotetrapods. After subjecting the AGaN network to about 20 loading-unloading cycles, the plastic component of the mechanical deformation has been removed and under further subsequent cycles, the aerogalnite architecture demonstrates high mechanical flexibility with rubber like elastic behaviour.

These excellent properties of AGaN are most likely due to its unique spatial architecture based on a mixture of micrometer-scale (length and diameter of aerotetrapod arms) and nanoscopic (thickness of the walls) features as well as due to elasticity, piezoelectricity and flexoelectricity. Flexoelectricity is negligible for bulk materials, while at the nanoscale it can be equal or even exceed the equivalent piezoelectricity [35]. Taking into account the nanoscale thickness of the walls of GaN hollow aerotetrapods and the mechanical bending inherent to tetrapod shape under compression [5], it is most likely that the flexoelectricity and

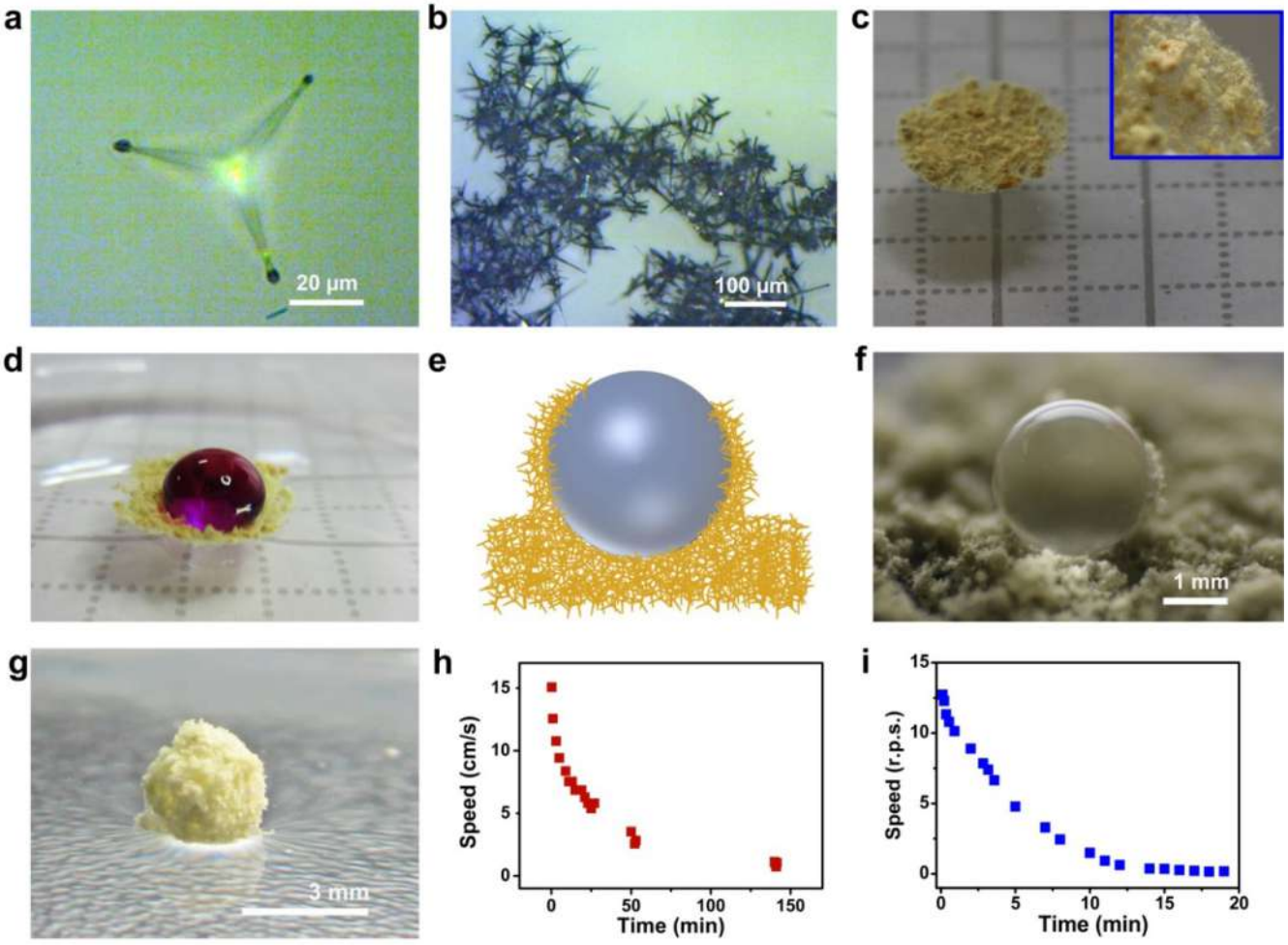

Fig. 4. AGaN tetrapod structures: (a) A single AGaN tetrapod floating on water. (b) A network of interpenetrating AGaN tetrapods floating on water. (c) An AGaN raft floating on water. (d) AGaN raft loaded with a drop of colored water. (e) Schematic illustration of encircling a water droplet by floating AGaN tetrapods. (f) A water droplet rolling onto an AGaN aerotetrapod bed. (g) Liquid droplet encapsulated by AGaN network. (h, i) Time dependences of the speed of translational and rotational motions of self-propelled AGaN liquid marbles, respectively.

piezoelectricity are cumulatively responsible with respect to the observed electromechanical response of aerogalnite. The previous investigations suggest that the yellow colour predominates in the light emission spectra of continuous and nanoperforated GaN membranes [36,37]. Besides, a strong yellow luminescence was also revealed in the near-surface layer of GaN nanowires as compared to weak yellow luminescence inherent to bulk [38]. Based on these findings, one may conclude that yellow colour centers are inherent to ultrathin membranes of gallium nitride, including AGaN which represents nanoscopically thin membranes shaped as hollow microtetrapods. It is necessary to mention that the ZnO traces exhibit negligible contribution to the luminescence of aerogalnite nanomaterial in the yellow region of the spectrum as confirmed by preliminary experiments.

3.2. Hydrophilic-hydrophobic behaviors

An individual AGaN aerotetrapod looks like an artificial pond skater [25] when placed on the surface of water (Fig. 4a). Interacting with the water in a similar way to the legs of a pond skater, the three down-positioned arms keep the microtetrapod floating on the water surface. By placing a big number of individual aerotetrapods on the water surface and inducing them to group together, one can weave a waterproof raft, see Fig. 4b. For weaving a flexible and mechanically durable AGaN raft, a 10-mm diameter sapphire cylinder was placed in a Petri dish partially filled in with water and aerotetrapods were gradually added on the water surface inside the sapphire cylinder, while the water bath with floating microtetrapods were simultaneously kept under ultrasound treatment. This resulted in the successful fabrication of a raft (digital image shown in Fig. 4c) out of interpenetrating AGaN aerotetrapod building blocks which covered the whole surface of the water inside the sapphire cylinder. The weaved raft was released (from the cylinder) by adding the sufficient amount of water to the Petri dish so to surpass the upper edge of the cylinder. Under these conditions the water surface inside the cylinder becomes convex, and the raft adopts the imposed geometrical shape, thus increasing its surface area by ~ 30% (Fig. S3, Supplementary Information). The AGaN raft is released when the threshold water level in the Petri dish is exceeded. Section 2 of the Video in the Supplementary Information illustrates the process of raft releasing and working principle of the raft via its force-displacement constitutive law (see details under the caption to Fig. S3 in the Supplementary Information), while a floating raft is shown in Fig. 4c. It is very important to highlight here that the imposed stretch in the process of releasing does not generate any ruptures in the AGaN raft which demonstrates its flexibility and pronounced stretching capabilities like in the nanoscale organic counterpart, the phospholipid bilayer of a cell membrane. In our opinion, the generated spatial architecture is durable because of the electrostatic interactions among the nanoscale-thick walls of neighboring aerotetrapods in the network. In

the weaved raft, the arms of the hollow aerotetrapods get deformed which induces electrical polarization of the walls owing to piezoelectric and flexoelectric phenomena.

The interaction between microtetrapods resembles the fascinating powerful grip of fire ants forming a raft during floods [26–28]. We found that an aerogalnite raft can carry liquid droplets hundreds of times heavier than the raft, i.e. it represents a micro-hydrofoil with impressive cargo capabilities. Fig. 4d illustrates a 0.37-mg weight raft carrying a liquid drop about 500 times heavier. It is important to note that, in the loading process, some AGaN rafts exhibited the capability of self-healing which is inherent to rafts formed by the fire ants [26,27]. Fig. S4a (Supplementary Information) illustrates the raft loading process, while Fig. S4b shows the maximum amount of liquid which can be carried by this AGaN micro-hydrofoil. When overloaded (i.e. when the admissible or the "threshold" amount of liquid is exceeded), the aerogalnite raft texture generates a hole which allows the leakage of a part of the colored liquid load (Fig. S4c). Raft self-healing seems to take place as soon as the overloading is removed, and the "self-repaired" micro-hydrofoil then continues to float, see Fig. S4(d-f). In most of our experiments with micro-hydrofoil loading we found, however, that as the liquid droplet increased in size it approached the raft border and rolled down into the water before reaching the "threshold" weight. Sections 3–5 of the Video (Supplementary Information) illustrate three consecutive processes of loading the same raft, each of them ending by droplet rolling down into the water. Directed flotation of both unloaded and loaded AGaN rafts can be easily actuated by applied static electric fields, see Sections 6,7 of the Video (Supplementary Information).

The investigation was extended to the consideration of a curved water surface, e.g., of a spherical surface. Consider a water droplet that keeps its spherical shape when encircled by floating pond skaters. We realized this concept by configuring AGaN microtetrapods as illustrated schematically in Fig. 4e: By rolling a water droplet onto a bed of AGaN microtetrapods (Fig. 4f), we reached full coverage of the droplet or, in other words, fabricated novel liquid marbles, see Fig. 4g. The liquid marbles represent aggregates composed of a drop of liquid encased in and stabilised by a shell of hydrophobic particles [39]. In our case the aerogalnite mimics the phospholipids bilayer that separates the inside and outside of biological cells as superhydrophobic separator, but with the advantage that the inorganic GaN material withstands extreme conditions such as high temperatures, harsh chemical environments and ultrasonic treatment.

The AGaN-based liquid marbles exhibit pronounced elasticity, as demonstrated in Section 8 of the Video (Supplementary Information) where a marble is subjected to a series of uniaxial compression-decompression cycles. Allowing a part of the liquid to evaporate through the porous shell, the mutual interpenetration of GaN microtetrapods is amplified and thus the AGaN shell is consolidated. Liquid marbles with consolidated AGaN shell are rather robust and survive, for example, on the surface of water subjected to intense ultrasonic treatment (Section 9 of the Video in Supplementary Information). The robustness of consolidated AGaN shells provides conditions for substantial modification of the shape of liquid marbles. Fig. S5 (Supplementary Information) shows an AGaN-based liquid marble exhibiting a visible deformation introduced by using a wood stick. Deviations from the spherical shape are of paramount importance for the development of self-propelled floating liquid marbles.

Recently, self-propelled liquid marbles have been fabricated using droplets of aqueous ethanol solutions encapsulated by fumed fluorosilica powder with 20–30 nm diameter particles [40] or by loose polytetrafluoroethylene particles with 1 μm diameter [41]. The occurrence of self-propulsion is related to Marangoni solutocapillary flow emerging when a gradient of surface tension of the fluid support is generated in the surrounding vicinity of the liquid marble. Such a gradient can be induced by breaking the spherical symmetry of the marbles. Under these conditions, the evaporation of alcohol, its condensation on the surrounding fluid surface and the resulting decrease in the surface tension prove to be spherically asymmetric, thus generating the solutocapillary effect. Taking this into account, we fabricated AGaN-based liquid marbles with various deviations from the spherical symmetry, the liquid droplets being composed of alcoholic solution. Section 10 of the Video (Supplementary Information) demonstrates a self-propelled AGaN-based floating liquid marble exhibiting mainly translational motion, while Fig. 4h illustrates the decrease of the marble speed with time. Although the maximum speed attained (15 cm/s) correlates with the speed reported by other groups for self-propelled liquid marbles, the lifetime of translational motion in our case proves to be more than 50 times longer than those reported previously (up to 2–3 min [40–42]). Taking into account that the reduction in motion of

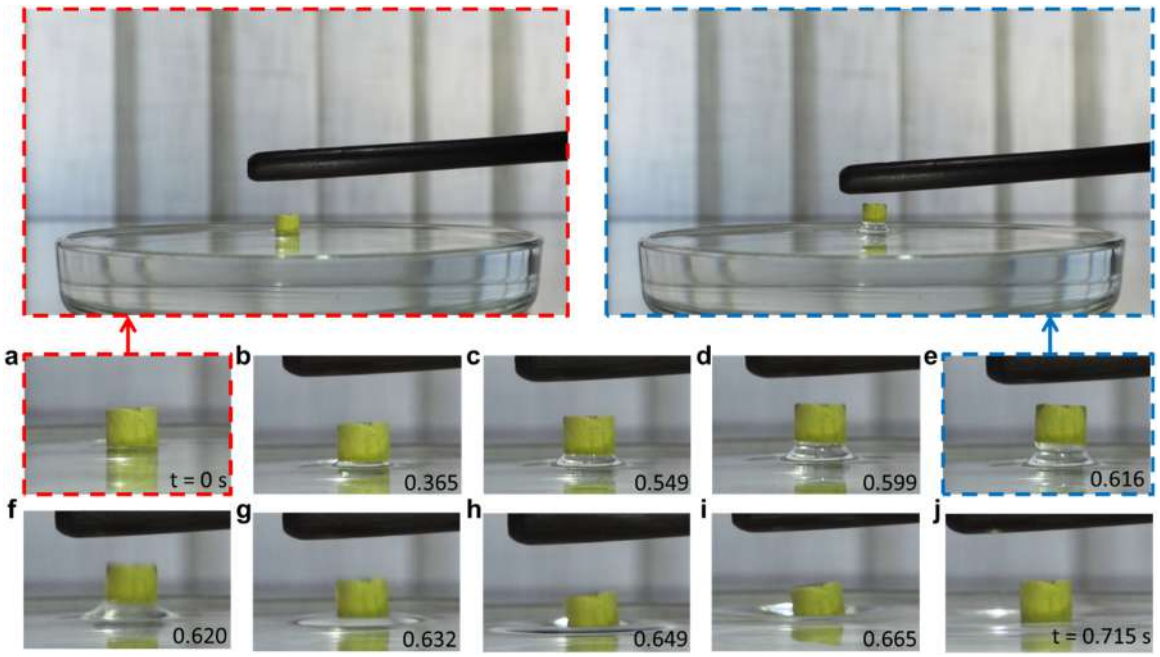

Fig. 5. A water pillar formed when a floating AGaN sample (equivalent to that shown in Fig. 1c) is lifted up by a charged amber stick.

liquid marbles is mainly due to water drag, it is evident that the effect of braking caused by the friction between AGaN shell and supporting fluid is relatively weak. The superhydrophobic-superhydrophilic combination of the AGaN provides marginal contact area and thus allows highly energy efficient motion.

The slight water drag is also revealed by the record rotational speed attained by the so-called *water tops* representing AGaN-based liquid marbles with specific deviations from the spherical symmetry. A self-propelled *water top* is illustrated by Section 11 of the Video (Supplementary Information). According to the results presented in Fig. 4i, the speed of rotation reaches values as high as 12.5 rot/sec which represents an impressive performance achieved by the self-propelled rotating liquid marbles. Note that, although the lifetime of rotational motion exceeds 15 min (Fig. 4i), it is much shorter than the lifetime of translational motion. This phenomenon is likely to be related to enhanced evaporation of volatile compounds from the liquid marble under conditions of circular hydrodynamic flow and outward centrifugal force emerging in the process of fast rotation [43].

The relatively slight water drag is likely to be a consequence of the spatial architecture of the AGaN shell. As one can see from Fig. 4a, due to the geometry of aerotetrapods only the free ends of their arms pierce through the water surface. Thus, between the AGaN shell and the water surface there is a layer of air crossed by super-hydrophobic tetrapod arms. The arms resemble clumps of hairs (four per clump) characteristic to the plant of *Salvinia molesta* which shows fascinating ability to keep submerged leaves coated with a thin layer of air and thus enabling the plant to carry out photosynthesis and gas exchange under-water [24]. In accordance with the results of recent investigations, the hairs of *Salvinia molesta* are topped by hydrophilic tips which pin the air-water interface and prevent rupture of contact [24,44]. Interestingly, similar phenomenon proves to be inherent to AGaN networks of tetrapods, i.e. the free ends of their arms are hydrophilic: they attract water. The hydrophilicity of the free ends of aerotetrapod arms can be explained considering that the arm closing plane coincides with polar crystallographic c-plane (note the similarity with phospholipid head based on polar phosphate groups). As a consequence of this, the surface tension pins the air-water interface to the free ends of the tetrapod arms.

The manifestation of water attachment to AGaN material observed in present experiments, aiming at the sample removal from the water surface, is again an important aspect to be briefly discussed. The time-lapse images presented in Fig. 5 (see also Supplementary Information, Section 12 of the Video) show how a water pillar is created when a floating AGaN sample is taken up by a charged amber stick. This demonstrates the phenomenon of water attachment or, in other words, how the free ends of the tetrapod arms touching the water surface pin the air-water interface. A schematic representation of the interface between water and hydrophilic free ends of AGaN tetrapod arms is illustrated in Fig. 6a where one can distinguish also a layer of air crossed by superhydrophobic tetrapod arms in the nearest proximity to the water surface. It is to be noted that even open microtubular arms appear to attract water due to the hydrophilicity of ZnO present on the inner surfaces of aerotetrapods, see Fig. 6b. Fig. 6b-e illustrate schematically the hydrophilicity of AGaN under tension and hydrophobicity when it is compressed against water for both open and closed microtubular arms. Due to dual hydrophilic-hydrophobic behaviour, the AGaN specimen skims over the water surface (see Section 12 of the Video in Supplementary Information) like a flying water lily beetle which is known to be tethered to the water by four hydrophilic claws, the rest of its body being hydrophobic and thus repelled by the water surface [23,24].

The detachment force of AGaN from the water surface was estimated by using the following strategy. A cylinder-shaped sample of AGaN (equivalent to that shown in Fig. 1c) was placed on one arm of two communicating vessels made from glass, while the other arm was used to pour water until it reached the surface of the highly porous AGaN specimen. Subsequently, the water was slowly removed from the free arm using a syringe. Fig. S6 and Section 13 of the Video (Supplementary Information) demonstrate how the AGaN specimen holds a 3-cm long water column attached to the bottom surface. In the experiment illustrated in Section 14 of the Video (Supplementary Information) the liquid was gradually removed from the right arm until it was detached from the bottom surface of the AGaN specimen in the left arm. Taking into account the difference in the water levels at the point of detachment and the inner diameter of communicating glass tubes (36 and 4 mm, respectively), the force of detachment was estimated to be as high as 4.4 mN (meaning a specific force or tensile strength σ_t of 35 mN/cm^2). It is interesting to note that a force of 4.4 mN can balance the gravitational attraction of ~60 aerogalnite samples equivalent to that shown in Fig. 1b (right).

In this experiment the force between aerogalnite sample and water is tensile. In this configuration, regardless to the nature of the tetrapod arm ends (open or close), the maximal tensile force per tip can be estimated as $F_{1,t} = 2\pi r\gamma\cos\theta_t$ (see Fig. 6b,c) where θ_t is the intrinsic contact angle of the tip (closed end) or of the internal wall (open end), r is the tetrapod radius (strictly speaking external or internal, respectively, see Fig. 6b,c) and γ is the liquid(-vapor) surface tension. Accordingly, the tensile strength of the tip is $\sigma_{1,t} = \frac{2\gamma}{r}\cos\theta_t$. This value can be estimated by the previous experiment as $\sigma_{1,t} = \frac{\sigma_t}{\varphi_a}$, where φ_a is the area fraction of the tetrapods in contact with water. The volume fraction of tetrapods in the aerogalnite is given by its density divided by the bulk density of GaN, i.e., $\varphi = \frac{\rho_{AGaN}}{\rho_{GaN}}$, resulting in a value of 0.002 ($\rho_{GaN} = 6150\frac{mg}{cm^3}$). Introducing the linear fractions $\varphi_{x,y,z}$ we can write $\varphi_a = \varphi_x\varphi_y$ and $\varphi = \varphi_x\varphi_y\varphi_z = \varphi_a\varphi_z$. For "cylindrical" porosity $\varphi_z = 1$ and $\varphi_a = \varphi$, whereas for "isotropic" porosity $\varphi_z = \varphi_y = \varphi_x$ and thus $\varphi_a = \varphi^{2/3}$, resulting in our case in $\varphi_a = 0.016$. Considering $\gamma = 0.07575\frac{N}{m}$ (distilled water) we can finally derive the intrinsic contact angle of the closed tips and internal walls as $\theta_t \cong 82°$ ($r \cong 1\mu$ m; note that assuming "cylindrical" rather than "isotropic" porosity –a much less realistic hypothesis– would not basically affect the prediction, yielding $\theta_t \cong 81°$). The

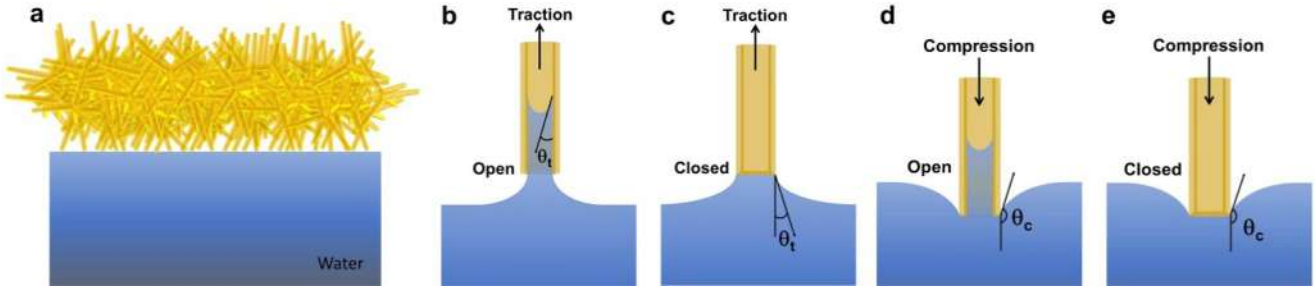

Fig. 6. (a) Illustration of an AGaN raft floating on water. (b-e) Schematic illustration of the combination of hydrophilic and hydrophobic properties inherent to closed or open ends of AGaN aerotetrapods in traction or compression.

apparent contact angle can be calculated by $\sigma_t = \frac{2\gamma}{R}\cos\theta_t^{(a)}$, where R is the sample radius in contact with water i.e., the internal radius of the glass vessel ($R \cong 0.4$ cm), fictitiously resulting in $\cos\theta_t^{(a)} \cong 9.24$ and thus physically $\theta_t^{(a)} = 0°$, i.e. aerogalnite in traction is perfectly superhydropilic and its tensile strength is further increased since ideally all the tetrapods in contact with water contribute to the overall adhesion force.

For completeness we can calculate the intrinsic contact angle θ_c of the core parts of the tetrapods; the observation of an apparent contact angle $\theta_c^{(a)}$ of about 170° suggests a Cassie-Baxter state and thus $\cos\theta_c^{(a)} = \varphi_a\cos\theta_c + \varphi_a - 1$, from where we derive $\cos\theta_c = -0.05$ and thus $\theta_c = 93°$, i.e., aerogalnite in compression is superhydrophobic thanks to the cumulative action of the individual tetrapods compressed against water (Fig. 6d,e) and of the air entrapped between them.

In the light of these results, one can qualitatively explain the record speed of rotation registered for the AGaN-based liquid marbles (Section 11 of the Video from the Supplementary Information). According to Fig. 4g, a liquid marble floats in a dimple formed on the water surface. From geometrical consideration, one can deduce that a limited number of the tetrapod arms touch the water surface in the dimple, see the schematic representation in Fig. S7, Supplementary information. Upon rotation of the liquid marble, the arm ends touching the liquid skim over its surface, thus resulting in a negligible water drag.

4. Conclusions

We developed an artificial nanomaterial made of hollow gallium nitride microtetrapods disclosing on their inner surfaces nanoscale traces of crystalline zinc oxide with outstanding chemical stability. The hydrophilicity of the nanoscale free ends and internal walls of the tetrapod arms as well as the hydrophobicity of the external GaN walls were demonstrated. Self-assembling tetrapods on the water surface enabled us to develop a proof-of-concept device, namely of stretchable and self-healing waterproof raft that uniquely exploits the dual hydrophilic-hydrophobic behaviors of the tetrapod networks and, as a result, manifest imposing cargo capabilities. Besides, we demonstrated highly energy efficient self-propelled liquid marbles exhibiting fast velocity of rotation and exceptional mechanical robustness (withstanding ultrasound). Strong interaction between hollow microtetrapods in the AGaN spatial networks, pronounced electromechanical coupling in three-dimensional architectures, unique combination of hydrophobic and hydrophilic characteristics along with biocompatibility [45–47] of gallium nitride nanostructures considerably broaden the scientific interest to this remarkable binary compound beyond traditional fields related to solid-state lighting technologies and high-frequency/high-power micro/nanoelectronics, and may open new avenues for its biomimetic applications in energy-efficient self-propelled micro-electro-mechanical structures, sensorics, microfluidics, microrobotics, medicine, etc. For instance, energy-efficient self-propelled liquid marbles based on AGaN can be used for controlling chemical reactions in confined space under conditions of rectilinear movement or rotation. Besides, liquid droplets coated by AGaN represent promising bioreactors for culturing cells, especially considering the high chemical stability and biocompatibility inherent to gallium nitride.

Acknowledgements

IT and TB acknowledge the support from the Academy of Sciences of Moldova under the Grants #15.817.02.29A, #17.820.5007.01 and #6222 (STCU). RA and LK acknowledge the support from Deutsche Forschungsgemeinschaft (DFG) under the scheme SFB 1261, TP {(A05, RA) & (A06, LK)}. RA thanks the DFG for the financial support via GRK 2154, Project P3. N.M.P. is supported by the FET Proactive "Neurofibres" grant No. 732344. This project has received funding from the European Union's Horizon 2020 research and innovation programme under grant agreement No 785219 (NMP: WP14 Composites; RA: WP13 "Functional Foams and Coatings"). NMP also acknowledge the support by the Italian Ministry of Education, University and Research (MIUR) under the “Departments of Excellence” grant no. L.232/ 2016.

Appendix A. Supporting information

Supplementary data associated with this article can be found in the online version at doi:10.1016/j.nanoen.2018.11.049

References

[1] S.J. Singer, G.L. Nicolson, The fluid mosaic model of the structure of cell membranes, Science 175 (1972) 720–731, https://doi.org/10.1126/science.175.4023.720.
[2] D.M. Engelman, Membranes are more mosaic than fluid, Nature 438 (2005) 578–580, https://doi.org/10.1038/nature04394.
[3] X. Jin, M. Götz, S. Wille, Y.K. Mishra, R. Adelung, C. Zollfrank, A novel concept for self-reporting materials: stress sensitive photoluminescence in ZnO tetrapod filled elastomers, Adv. Mater. 25 (2013) 1342–1347, https://doi.org/10.1002/adma.201203849.
[4] S.N. Raja, A.C.K. Olson, K. Thorkelsson, A.J. Luong, L. Hsueh, G. Chang, B. Gludovatz, L. Lin, T. Xu, R.O. Ritchie, A.P. Alivisatos, Tetrapod nanocrystals as fluorescent stress probes of electrospun nanocomposites, Nano Lett. 13 (2013) 3915–3922, https://doi.org/10.1021/nl401999t.
[5] R. Meija, S. Signetti, A. Schuchardt, K. Meurisch, D. Smazna, M. Mecklenburg, K. Schulte, D. Erts, O. Lupan, B. Fiedler, Y.K. Mishra, R. Adelung, N.M. Pugno, Nanomechanics of individual aerographite tetrapods, Nat. Commun. 8 (2017) 14982, https://doi.org/10.1038/ncomms14982.
[6] L. Manna, D.J. Milliron, A. Meisel, E.C. Scher, A.P. Alivisatos, Controlled growth of tetrapod branched inorganic nanocrystals, Nat. Mater. 2 (2003) 382–385, https://doi.org/10.1038/nmat902.
[7] Y.K. Mishra, R. Adelung, ZnO tetrapod materials for functional applications, Mater. Today 21 (2018) 631–651, https://doi.org/10.1016/j.mattod.2017.11.003.
[8] M.S. Kang, C.-H. Lee, J.B. Park, H. Yoo, G.-C. Yi, Gallium nitride nanostructures for light-emitting diode applications, Nano Energy 1 (2012) 391–400, https://doi.org/10.1016/J.NANOEN.2012.03.005.
[9] X. Wang, W. Peng, R. Yu, H. Zou, Y. Dai, Y. Zi, C. Wu, S. Li, Z.L. Wang, Simultaneously enhancing light emission and suppressing efficiency droop in GaN microwire-based ultraviolet light-emitting diode by the piezo-phototronic effect, Nano Lett. 17 (2017) 3718–3724, https://doi.org/10.1021/acs.nanolett.7b01004.
[10] M. Peng, Y. Liu, A. Yu, Y. Zhang, C. Liu, J. Liu, W. Wu, K. Zhang, X. Shi, J. Kou, J. Zhai, Z.L. Wang, Flexible self-powered GaN ultraviolet photoswitch with piezo-phototronic effect enhanced on/off ratio, ACS Nano 10 (2016) 1572–1579, https://doi.org/10.1021/acsnano.5b07217.
[11] X. Wang, R. Yu, W. Peng, W. Wu, S. Li, Z.L. Wang, Temperature dependence of the piezotronic and piezophototronic effects in a -axis GaN nanobelts, Adv. Mater. 27 (2015) 8067–8074, https://doi.org/10.1002/adma.201504534.
[12] J. Zhang, S.A. Meguid, On the piezoelectric potential of gallium nitride nanotubes, Nano Energy 12 (2015) 322–330, https://doi.org/10.1016/J.NANOEN.2014.12.036.
[13] C.H. Wang, W.S. Liao, Z.H. Lin, N.J. Ku, Y.C. Li, Y.C. Chen, Z.L. Wang, C.P. Liu, Optimization of the output efficiency of GaN nanowire piezoelectric nanogenerators by tuning the free carrier concentration, Adv. Energy Mater. 4 (2014) 1400392, https://doi.org/10.1002/aenm.201400392.
[14] S.-J. Tsai, C.-Y. Lin, C.-L. Wang, J.-W. Chen, C.-H. Chen, C.-L. Wu, Efficient coupling of lateral force in GaN nanorod piezoelectric nanogenerators by vertically integrated pyramided Si substrate, Nano Energy 37 (2017) 260–267, https://doi.org/10.1016/J.NANOEN.2017.05.033.
[15] X. Wen, W. Wu, C. Pan, Y. Hu, Q. Yang, Z. Lin Wang, Development and progress in piezotronics, Nano Energy 14 (2015) 276–295, https://doi.org/10.1016/J.NANOEN.2014.10.037.
[16] M. Dragoman, L. Ghimpu, C. Obreja, A. Dinescu, I. Plesco, T. Braniste, I. Tiginyanu, Ultra-lightweight pressure sensor based on graphene aerogel decorated with piezoelectric nanocrystalline films, Nanotechnology 27 (2016) 475203, https://doi.org/10.1088/0957-4484/27/47/475203.
[17] M. Mecklenburg, A. Schuchardt, Y.K. Mishra, S. Kaps, R. Adelung, A. Lotnyk, L. Kienle, K. Schulte, Aerographite: ultra lightweight, flexible nanowall, carbon microtube material with outstanding mechanical performance, Adv. Mater. 24 (2012) 3486–3490, https://doi.org/10.1002/adma.201200491.
[18] A. Schuchardt, T. Braniste, Y.K. Mishra, M. Deng, M. Mecklenburg, M.A. Stevens-Kalceff, S. Raevschi, K. Schulte, L. Kienle, R. Adelung, I. Tiginyanu, Three-dimensional Aerographite-GaN hybrid networks: single step fabrication of porous and mechanically flexible materials for multifunctional applications, Sci. Rep. 5 (2015) 8839, https://doi.org/10.1038/srep08839.
[19] Y.K. Mishra, S. Kaps, A. Schuchardt, I. Paulowicz, X. Jin, D. Gedamu, S. Freitag, M. Claus, S. Wille, A. Kovalev, S.N. Gorb, R. Adelung, Fabrication of macroscopically flexible and highly porous 3D semiconductor networks from interpenetrating nanostructures by a simple flame transport approach, Part. Part. Syst. Charact. 30 (2013) 775–783, https://doi.org/10.1002/ppsc.201300197.
[20] F. Schütt, S. Signetti, H. Krüger, S. Röder, D. Smazna, S. Kaps, S.N. Gorb,

Y.K. Mishra, N.M. Pugno, R. Adelung, Hierarchical self-entangled carbon nanotube tube networks, Nat. Commun. 8 (2017) 1215, https://doi.org/10.1038/s41467-017-01324-7.
[21] J. Goldberger, R.R. He, Y.F. Zhang, S.W. Lee, H.Q. Yan, H.J. Choi, P.D. Yang, Single-crystal gallium nitride nanotubes, Nature 422 (2003) 599–602, https://doi.org/10.1038/nature01484.1.
[22] S.B. Thapa, J. Hertkorn, T. Wunderer, F. Lipski, F. Scholz, A. Reiser, Y. Xie, M. Feneberg, K. Thonke, R. Sauer, M. Dürrschnabel, L.D. Yao, D. Gerthsen, H. Hochmuth, M. Lorenz, M. Grundmann, MOVPE growth of GaN around ZnO nanopillars, J. Cryst. Growth 310 (2008) 5139–5142, https://doi.org/10.1016/j.jcrysgro.2008.07.009.
[23] H. Mukundarajan, T.C. Bardon, D.H. Kim, M. Prakash, Surface tension dominates insect flight on fluid interfaces, J. Exp. Biol. 219 (2016) 752–766, https://doi.org/10.1242/jeb.127829.
[24] E. Pennisi, Water's tough skin, Science 343 (2014) 1194–1197, https://doi.org/10.1126/science.343.6176.1194.
[25] D.L. Hu, B. Chan, J.W.M. Bush, The hydrodynamics of water strider locomotion, Nature 424 (2003) 663–666, https://doi.org/10.1038/nature01793.
[26] M. Tennenbaum, Z. Liu, D. Hu, A. Fernandez-nieves, Mechanics of fire ant aggregations, Nat. Mater. 15 (2016) 54–59, https://doi.org/10.1038/nmat4450.
[27] P.C. Foster, N.J. Mlot, A. Lin, D.L. Hu, Fire ants actively control spacing and orientation within self-assemblages, J. Exp. Biol. 217 (2014) 2089–2100, https://doi.org/10.1242/jeb.093021.
[28] N.J. Mlot, C.A. Tovey, D.L. Hu, Fire ants self-assemble into waterproof rafts to survive floods, Proc. Natl. Acad. Sci. USA 108 (2011) 7669–7673, https://doi.org/10.1073/pnas.1016658108.
[29] Y. Si, J. Yu, X. Tang, J. Ge, B. Ding, Ultralight nanofibre-assembled cellular aerogels with superelasticity and multifunctionality, Nat. Commun. 5 (2014) 5802, https://doi.org/10.1038/ncomms6802.
[30] R. Pethig, Review article—dielectrophoresis: status of the theory, technology, and applications, Biomicrofluidics 4 (2010) 022811, https://doi.org/10.1063/1.3456626.
[31] H. Sowa, H. Ahsbahs, High-pressure X-ray investigation of zincite ZnO single crystals using diamond anvils with an improved shape, J. Appl. Crystallogr. 39 (2006) 169–175, https://doi.org/10.1107/S0021889805042457.
[32] A.F. Wright, J.S. Nelson, Consistent structural properties for AlN, GaN, and InN, Phys. Rev. B 51 (1995) 7866–7869, https://doi.org/10.1103/PhysRevB.51.7866.
[33] Y. Ding, Z.L. Wang, Structures of planar defects in ZnO nanobelts and nanowires, Micron 40 (2009) 335–342, https://doi.org/10.1016/j.micron.2008.10.008.
[34] D.N. Zakharov, Z. Liliental-Weber, B. Wagner, Z.J. Reitmeier, E.A. Preble, R.F. Davis, Structural TEM study of nonpolar a-plane gallium nitride grown on (1120) 4H-SiC by organometallic vapor phase epitaxy, Phys. Rev. B 71 (2005), https://doi.org/10.1038/ncomms6802.
[35] T.D. Nguyen, S. Mao, Y.W. Yeh, P.K. Purohit, M.C. McAlpine, Nanoscale flexoelectricity, Adv. Mater. 25 (2013) 946–974, https://doi.org/10.1002/adma.201203852.
[36] I.M. Tiginyanu, V. Popa, M.A. Stevens-Kalceff, D. Gerthsen, P. Brenner, D. Pavlidis, Design and maskless fabrication of ultrathin suspended membranes of GaN, Phys. Status Solidi - Rapid Res. Lett. 4 (2012) 148–150, https://doi.org/10.1002/pssr.201206020.
[37] O. Volciuc, T. Braniste, I. Tiginyanu, M.A. Stevens-Kalceff, J. Ebeling, T. Aschenbrenner, D. Hommel, V. Ursaki, J. Gutowski, The impact of nano-perforation on persistent photoconductivity and optical quenching effects in suspended GaN nanomembranes, Appl. Phys. Lett. 103 (2013) 243113, https://doi.org/10.1063/1.4847735.
[38] Q. Li, G.T. Wang, Spatial distribution of defect luminescence in GaN nanowires, Nano Lett. 10 (2010) 1554–1558, https://doi.org/10.1021/nl903517t.
[39] P. Aussillous, D. Quéré, Liquid marbles, Nature 411 (2001) 924–927, https://doi.org/10.1038/35082026.
[40] E. Bormashenko, Y. Bormashenko, R. Grynyov, H. Aharoni, G. Whyman, B.P. Binks, Self-propulsion of liquid marbles: leidenfrost-like levitation driven by marangoni flow, J. Phys. Chem. C 119 (2015) 9910–9915, https://doi.org/10.1021/acs.jpcc.5b01307.
[41] C.H. Ooi, A. van Nguyen, G.M. Evans, O. Gendelman, E. Bormashenko, N.-T. Nguyen, A floating self-propelling liquid marble containing aqueous ethanol solutions, RSC Adv. 5 (2015) 101006–101012, https://doi.org/10.1039/C5RA23946J.
[42] E. Bormashenko, Liquid marbles, elastic nonstick droplets: from minireactors to self-propulsion, Langmuir 33 (2017) 663–669, https://doi.org/10.1021/acs.langmuir.6b03231.
[43] X. Han, H.K. Lee, Y.H. Lee, X.Y. Ling, Dynamic rotating liquid marble for directional and enhanced mass transportation in three-dimensional microliter droplets, J. Phys. Chem. Lett. 8 (2017) 243–249, https://doi.org/10.1021/acs.jpclett.6b02743.
[44] W. Barthlott, T. Schimmel, S. Wiersch, K. Koch, M. Brede, M. Barczewski, S. Walheim, A. Weis, A. Kaltenmaier, A. Leder, H.F. Bohn, The salvmia paradox: superhydrophobic surfaces with hydrophilic pins for air retention under water, Adv. Mater. 22 (2010) 2325–2328, https://doi.org/10.1002/adma.200904411.
[45] T. Braniste, I. Tiginyanu, T. Horvath, S. Raevschi, S. Cebotari, M. Lux, A. Haverich, A. Hilfiker, Viability and proliferation of endothelial cells upon exposure to GaN nanoparticles, Beilstein J. Nanotechnol. 7 (2016) 1330–1337, https://doi.org/10.3762/bjnano.7.124.
[46] T. Braniste, I. Tiginyanu, T. Horvath, S. Raevschi, B. Andrée, S. Cebotari, E.C. Boyle, A. Haverich, A. Hilfiker, Targeting endothelial cells with multifunctional GaN/Fe nanoparticles, Nanoscale Res. Lett. 12 (2017) 486, https://doi.org/10.1186/s11671-017-2262-y.
[47] S.Y. Lee, K.-I. Park, C. Huh, M. Koo, H.G. Yoo, S. Kim, C.S. Ah, G.Y. Sung, K.J. Lee, Water-resistant flexible GaN LED on a liquid crystal polymer substrate for implantable biomedical applications, Nano Energy 1 (2012) 145–151, https://doi.org/10.1016/J.NANOEN.2011.07.001.

Ion Tiginyanu received his Ph.D. degree in Semiconductor Physics from Lebedev Institute of Physics, Moscow, in 1982. Starting from 2001, he serves as the founding Director of the National Center for Materials Study and Testing, Technical University of Moldova. In 2013 he was elected first vice-president of the Academy of Sciences of Moldova. Professor Tiginyanu's research interests are related to nanotechnologies, smart nanomaterials and development of photonic and electronic novel device structures. He is SPIE Fellow, senior member of OSA, and member of AAAS, MRS, IEEE, and the Electrochemical Society. More information is available at www.ncmst.utm.md.

Tudor Braniste received his Ph.D. degree in nano-microelectronics and optoelectronics from the Technical University of Moldova (TUM) in 2017. During his PhD studies he held a DAAD scholarship at Hannover Medical School, Germany, where he studied the biocompatibility of GaN nanoparticles and their interaction with endothelial cells. Since 2017 he is a researcher at TUM and his current research interests include bio-nanotechnologies related to wide bandgap semiconductors, nanotechnologies based on self-assembling, chemical and electrochemical etching, sensors, etc. More information is available at www.ncmst.utm.md.

Daria Smazna, Donetsk (Ukraine), 03.10.1989. She received her Master's degree in Material Science and Engineering in 2013 at Kiel University, Germany, and her Bachelor and Master degree in Electrical Engineering at Donetsk National University in 2010 and 2011, respectively. Since 2013, she works as a PhD student at the Material Science department of the CAU Kiel in the research group of Prof. Dr. Adelung. Her research interests are functionalization of semiconducting nano- and microstructures for enhanced sensing, conducting and bio- applications.

Mao Deng (Ph.D.) studied Material Chemistry at the Sichuan University China for Bachelor degree and Master degree in Material Science & Engineering at Kiel University, Germany. Afterward, Mao started professional activity as a scientific researcher at Kiel University where she focused on nanomaterial analysis using electron microscopy. Particularly, she studied the determination and simulation for crystal structure and chemical bonding states of catalysts, nano-sensors, biomaterials and nanocomposites. Besides her interdisciplinary projects, she was also responsible for the installation and operation of TEM for the application in nano-texture determination and electron spectroscopy.

Fabian Schütt, born in 1989, is working since 2014 as a PhD student at the Chair for Functional Nanomaterials (Prof. Dr. Rainer Adelung) at the Institute for Materials Science, Faculty of Engineering, Kiel University, Germany. In the framework of his PhD he developed new methods for the synthesis of highly porous aeromaterials, which he characterized and applied in different application fields. His current research is focused on the utilisation of nanoscopic functionality of low dimensional nanomaterials, such as graphene, carbon nanotubes or hexagonal boron nitride in macroscopically expanded framework structures.

Arnim Schuchardt completed his Ph.D. at the Chair for Functional Nanomaterials, Prof. Dr. Adelung, at Kiel University, Germany. For his Ph.D. he worked in the field of 3D interconnected ZnO networks and its conversion to 3D cellular Aerographitic networks. In the research of Aerographite his focus was the electrical and mechanical characterization as well as the development of appropriate test setups. Currently he is working in the field of FEM and CFD simulations in the automotive industry at Bosch/AE.

Marion Stevens-Kalceff (PhD) is an experimental condensed matter physicist with research interests including the defect structure of wide band gap materials, electron beam-condensed matter interactions, irradiation induced microstructural defect generation and transformation of the defect structure of wide band gap materials and their microcharacterization using SEM based cathodoluminescence spectroscopy and imaging techniques. This work was done while Marion Stevens-Kalceff was an Associate Professor in the School of Physics at the University of New South Wales, Sydney, Australia.

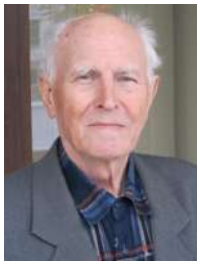

Simion Raevschi received his Ph.D. degree in Technical Sciences from the Moscow Institute of Scientific Research, Design and Technology of Current Sources in 1976. Since 1984 he works as a researcher in the Experimental Physics Department of the State University of Moldova. His research interests are focused on the development of cost-effective technologies for epitaxial growth of III-V compounds on homogeneous and heterogeneous substrates by using chemical transport reactions.

Ulrich Schürmann (PhD) studied mineralogy at Kiel University (1995–2001) and conducted his diploma thesis in 2001. From 2001 to 2006, he was working at the Chair for “Multicomponent Materials” of Prof. F. Faupel at the Institute for Materials Science and obtained his Ph.D. degree on co-sputtering of polymer-silver-nanocomposites. He was Postdoc at Caesar in Bonn (2006–2007) and in the groups “Inorganic Functional Materials” (2007–2009) and “Synthesis and Real Structure” (since 2009) at the Institute for Materials Science at Kiel University. Since 2011, he is coordinator of the TEM Center at the Faculty of Engineering, Kiel Univeristy..

Lorenz Kienle is Professor for Synthesis and Real Structure at the Faculty of Engineering of the Kiel University, Germany. Moreover he is heading the center for TEM at the Faculty of Engineering. His research focuses on the synthesis of novel bulk- and nanomaterials by chemical approaches and thin film deposition techniques as well as characterization by state of the art nanoanalytical methods, including TEM, XRD and others. Presently the materials under investigation are chemical and magnetic-field sensors, thermoelectrics, battery materials, complex alloy nanoparticles, piezoelectrics and superlattice nanostructures.

Nicola M. Pugno, born in 1972; Master's degrees in Engineering and Physics (both cum laude); PhD degrees in Engineering and Biology; Professor of Solids and Structural Mechanics at the University of Trento and there Director of the Laboratory of Bio-Inspired and Graphene Nanomechanics since 2012 as well as Professor of Materials Science at the Queen Mary University of London since 2013 (part-time); first Editor-in-Chief of Frontiers in Materials and its section on Mechanics; Winner of 4 ERC (1 StG and 3 PoC) and other EU grants (e.g. task leader within the Graphene Flagship for composites modelling) and of the Griffith Medal and Prize 2017. See details at http://www.ing.unitn.it/~pugno/

Yogendra Kumar Mishra (Privat Dozent) is leading a Group with focus on 3D Nanomaterials at the Chair for Functional Nanomaterials, Institute for Materials Science, Kiel University, Germany. After Ph.D. (Physics, 2008) from JNU New Delhi, India, he migrated to Kiel as Humboldt Fellow (2009–2011) and subsequently continued as group leader at Functional Nanomaterials. In Kiel, he introduced a new technique called Flame Transport Synthesis which allows versatile nanostructuring of metal oxide tetrapods based 3D networks. These networks can be used as sacrificial templates to develop new 3D interconnected materials from metals, carbons, oxides, nitrides, etc. opening large scopes towards advanced technologies.

Rainer Adelung is full professor and Chairholder of the Functional Nanomaterials established in 2007 at the Institute for Materials Science, Kiel University, Germany. He received his Ph.D. (rer. nat.) in physics in 2000 from the Institute of Experimental and Applied Physics, Kiel University, and during 2001–2002 he was at Case Western Reserve University in Cleveland (USA) as Feodor Lynen (Alexander von Humboldt) research fellow. In 2006 he finished his Habilitation at the Institute for Materials Science in Kiel and then continued as Heisenberg Professor (DFG grant) with his own Functional Nanomaterials group in 2012. More information is available at http://fnano.matwis.tf.uni-kiel.de/.

Supporting Information

Self-organized and self-propelled aero-GaN with dual hydrophilic-hydrophobic behavior

Ion Tiginyanu[a,b,c]*, Tudor Braniste[b], Daria Smazna[a], Mao Deng[a], Fabian Schütt[a], Arnim Schuchardt[a], Marion A. Stevens-Kalceff[d], Simion Raevschi[e], Ulrich Schürmann[a], Lorenz Kienle[a], Nicola M. Pugno[f,g,h], Yogendra Kumar Mishra[a]*, Rainer Adelung[a]*

[a]Institute for Materials Science, Kiel University, Kaiserstr. 2, D-24143 Kiel, Germany
[b]National Center for Materials Study and Testing, Technical University of Moldova, Stefan cel Mare av. 168, MD-2004 Chisinau, Moldova
[c]Academy of Sciences of Moldova, Stefan cel Mare av. 1, MD-2001 Chisinau, Moldova
[d]School of Physics, University of New South Wales, NSW 2052 Sydney, Australia
[e]Department of Physics and Engineering, State University of Moldova, Alexei Mateevici str. 60, MD-2009 Chisinau, Moldova
[f]Laboratory of Bio-Inspired and Graphene Nanomechanics, Department of Civil, Environmental and Mechanical Engineering, University of Trento, 38123 Trento, Italy
[g]School of Engineering and Materials Science, Queen Mary University of London, Mile End Road, E1 4NS London, United Kingdom
[h]Ket Lab, Edoardo Amaldi Foundation, Italian Space Agency, Via del Politecnico snc, 00133 Rome, Italy

Corresponding authors:
IT (tiginyanu@asm.md)
YKM (ykm@tf.uni-kiel.de)
RA (ra@tf.uni-kiel.de)

Keywords: Gallium nitride; hollow tetrapods; 3D network; self-assembling tetrapods on water; hydrophobic wetting; hydrophilic dewetting.

Figure S1

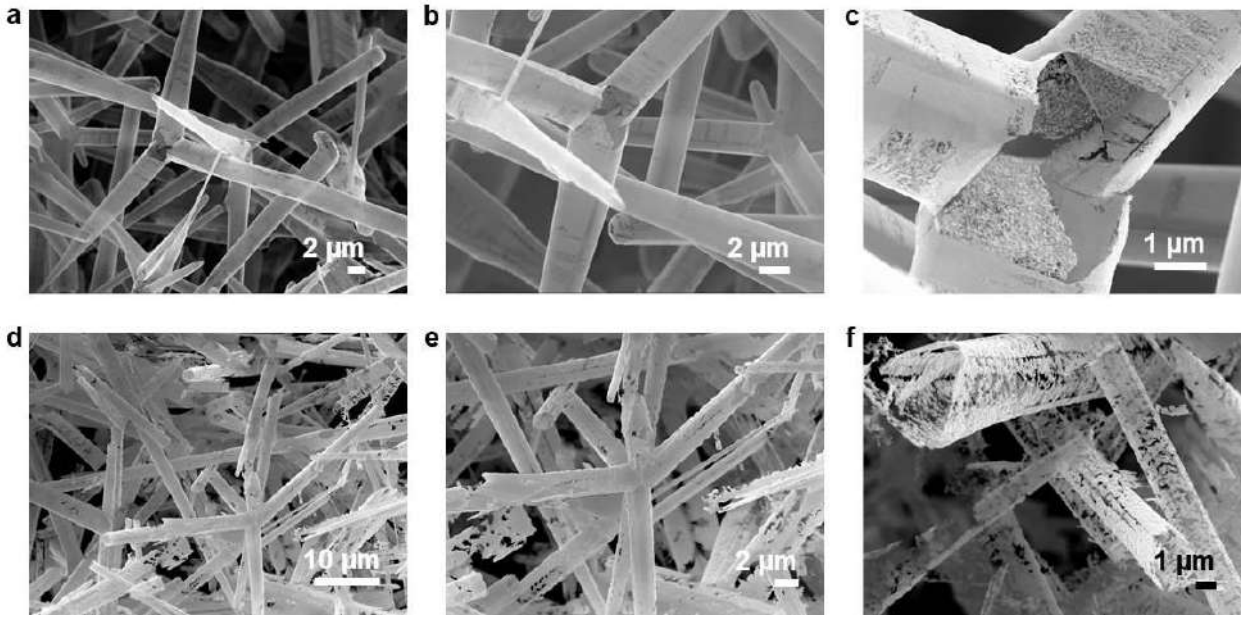

Figure S1. SEM images taken from AGaN samples grown at T_g: (a-c) 900°C; (d-f) 950°C.

Figure S2

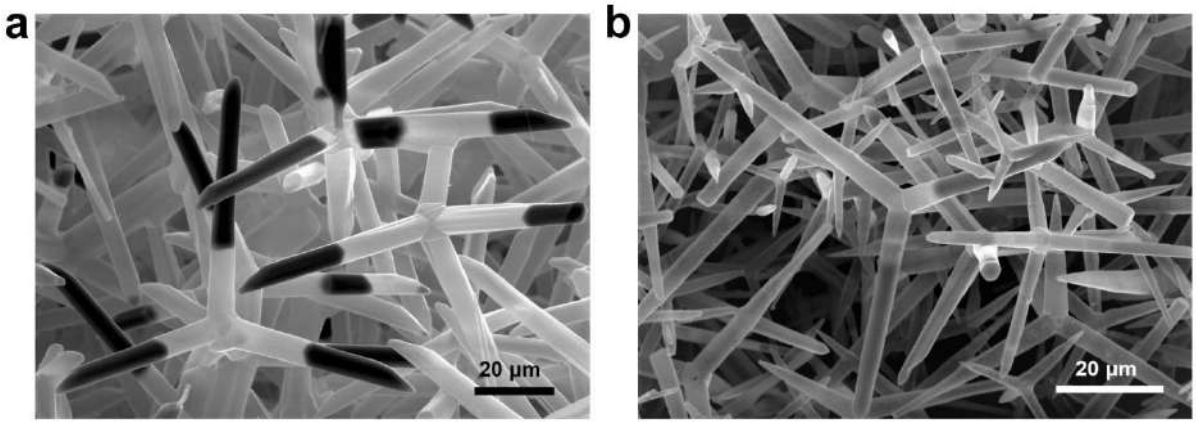

Figure S2. SEM images taken from AGaN samples which show partial removal of ZnO in the process of GaN deposition using HVPE.

Figure S3

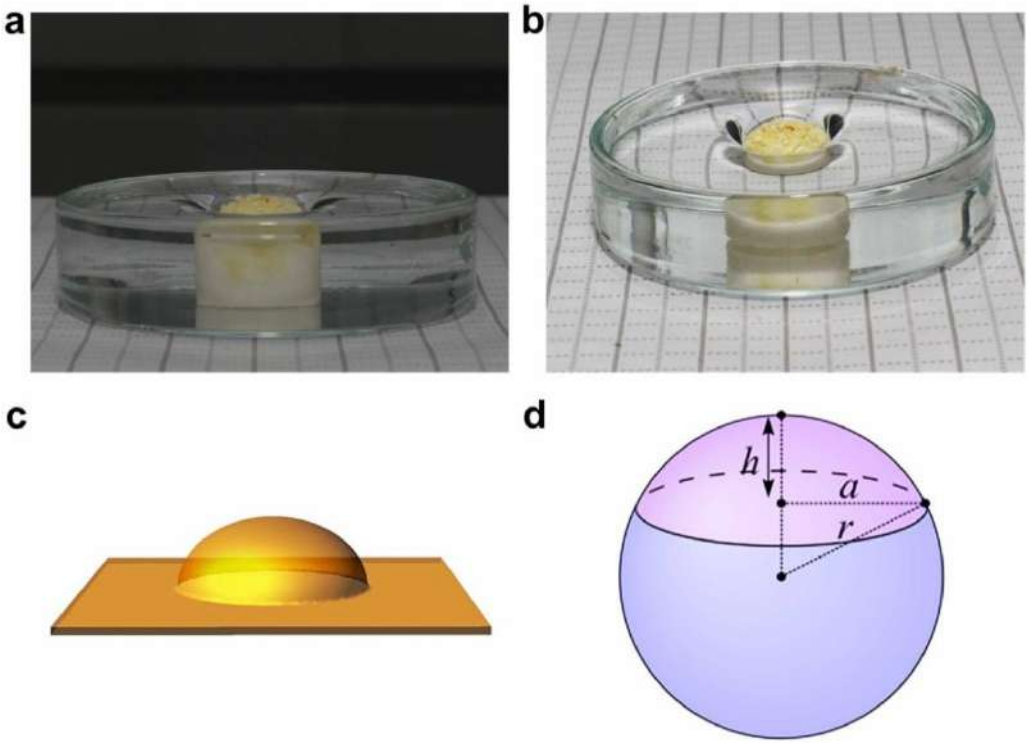

Figure S3. (a) and (b) The imposed stretch in the process of raft release, see details in Section 2 from the Video, see Supplementary Information; (c) spherical cap emerging in the process of AGaN raft release and (d) parameters used in the calculation of the lateral surface of the spherical cap.

Surface of spherical cap

Initial surface of the circular area:

$A_i=\pi*a^2=3.14*5.5^2=94.98$ mm^2

The lateral surface of the spherical cap was calculated according to the following formula:

$A_l=\frac{\pi}{4}[(2a)^2+4h^2]=\frac{3.14}{4}*\left[(2*5.5)^2+4*3^2\right]=123.2$ mm^2

where,

a – is the radius of the circle;

h – the height of the spherical cap emerging in the process of AGaN raft release.

Working principle of the raft: force-displacement constitutive law

The downward external force F applied on the raft plus its weight is counterbalanced by capillary and buoyancy, i.e. the constitutive law that we have observed in the floating experiment can be rationalized with:

$F(d)=-\rho gtA-P\gamma cos\theta_c^{(a)}+\rho_l gAd$

where ρ,t,A,P are respectively density, thickness, surface area and perimeter (in contact with water) of the raft, ρ_l is the liquid (water) density and $d=V/A$ is the "nominal" depth of the dimple defined via its total (including raft) volume V.

Figure S4

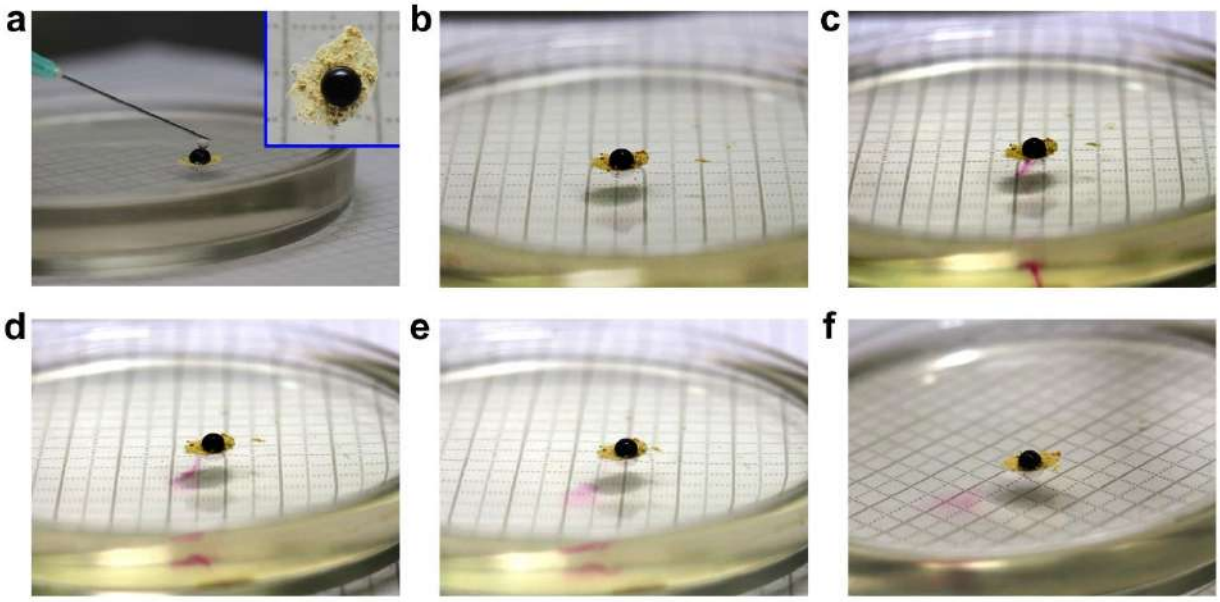

Figure S4. Illustration of the raft loading process (a), maximum admissible load (b), leakage of some colored liquid (c) and further floating of the AGaN raft after self-healing (d,e,f).

Figure S5

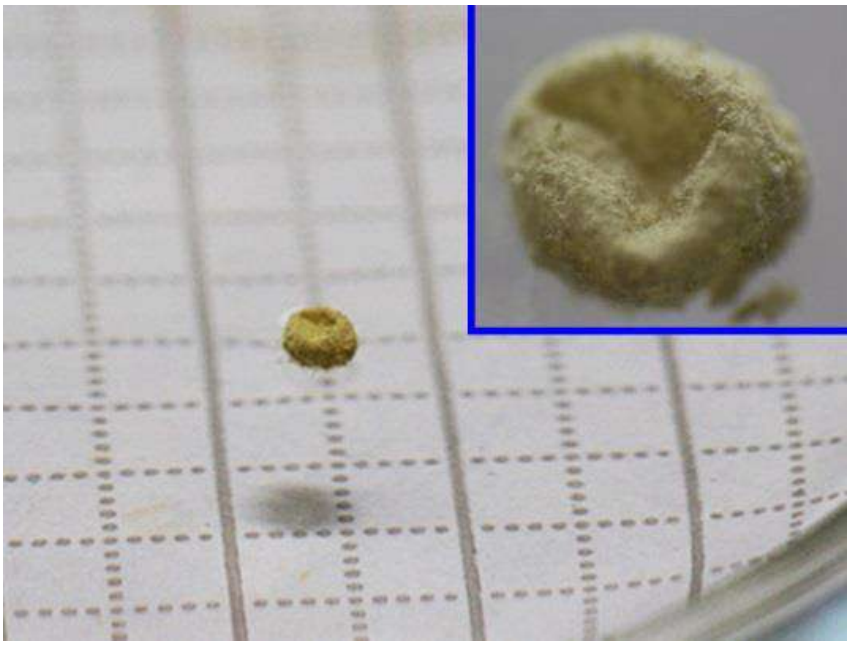

Figure S5. A liquid marble with a shape deviating from the spherical.

Figure S6

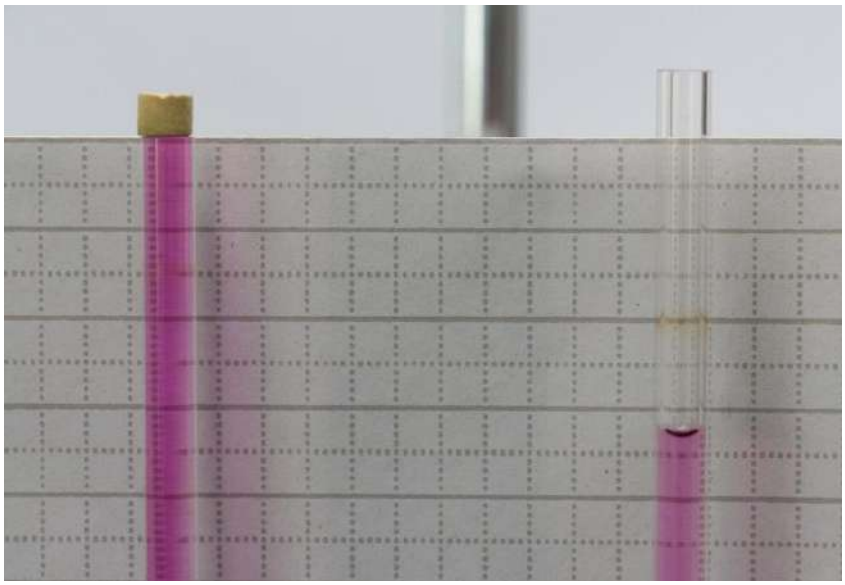

Figure S6. Digital image of the AGaN specimen holding a 3-cm long water column attached to the bottom surface in the left arm of communicating vessels.

Figure S7

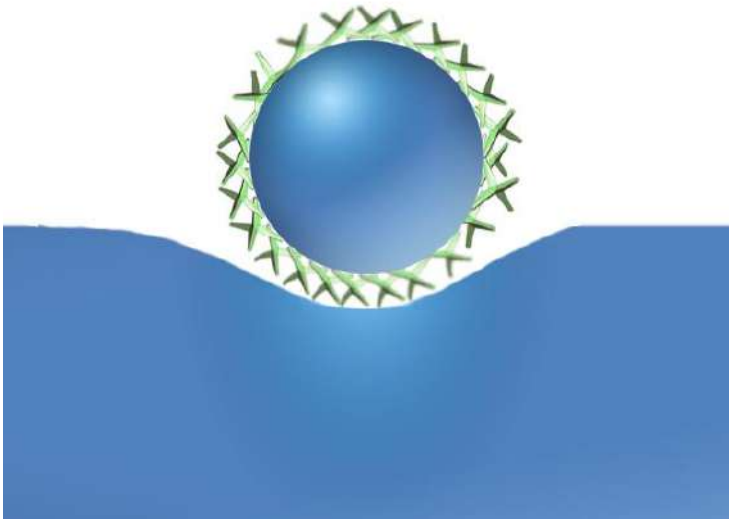

Figure S7. Schematic representation of an AGaN-based liquid marble floating on water.